Available online at www.sciencedirect.com
ScienceDirect
Journal of the European Ceramic Society 29 (2009) 1139–1146
www.elsevier.com/locate/jeurceramsoc

Doping effect on secondary phases, microstructure and electrical conductivities of $LaGaO_3$ based perovskites

Shuai Li *, Bill Bergman

Department of Materials Science and Engineering, School of Industrial Engineering and Management, Royal Institute of Technology, SE 10044 Stockholm, Sweden

Received 14 April 2008; received in revised form 6 August 2008; accepted 12 August 2008
Available online 26 September 2008

Abstract

The intermediate temperature electrolytes $La_{1-x}Sr_xGa_{1-y}Mg_yO_{3-\delta}$ (LSGM, where $\delta=(x+y)/2$) with perovskite structure were prepared using a poly(vinyl alcohol) (PVA) solution polymerization method. Three secondary phases were identified by X-ray diffraction, $LaSrGaO_4$, $LaSrGa_3O_7$ and $La_4Ga_2O_9$. The relative amount of these secondary phases depended on the doping compositions. Sr doping produced more Sr rich secondary phases with increasing content, while enhanced solid solubility was observed with Mg addition. Sintered samples showed dense microstructures with well-developed equiaxed grains, and the secondary phases were mainly in the grain boundaries. $LaSrGaO_4$ could not be detected by SEM for the sintered pellets. The oxygen ionic conductivity was enhanced by doping with Sr and Mg. Mg doping showed the increased conductivity activation energy. $La_{0.8}Sr_{0.2}Ga_{0.9}Mg_{0.1}O_{2.85}$ had the highest ionic conductivity $\sigma=0.128$ S/cm at 800 °C in this work.

Keywords: Perovskite; Lanthanum gallate; Secondary phases; Microstructure; Ionic conductivity

1. Introduction

Solid oxide fuel cells (SOFCs) convert chemical energy of the fuel directly to electrical energy with high efficiency and are environmentally friendly.[1] Typical SOFCs with yttria-stabilized-zirconia (YSZ) electrolytes require high operating temperatures (800–1000 °C). The high temperature may cause serious problems for sealing materials, thermal mismatches and reaction between interface materials, leading to higher manufacturing cost and application limitation.[2] Therefore, effect has been focused on developing and designing novel oxide electrolytes which can operate at intermediate temperatures (500–800 °C). Stabilized Bi_2O_3 and doped CeO_2 show higher conductivity than YSZ at low temperatures and should thus be interesting alternatives. But later works showed that CeO_2 and Bi_2O_3 based oxides become mixed electronic/oxide-ion conductors in the reducing atmosphere.[3] In 1994, Ishihara et al.[4] and Feng and Goodenough[5] reported that the perovskite $LaGaO_3$ doped with Sr and Mg had an oxide ion conductivity $\sigma>0.10$ S/cm at 800 °C, which exceeded those of YSZ by a factor of about three. Moreover, the materials had a near unity transference number in the oxygen partial pressure region from 10^{-22} to 1 atm and showed a stable performance over long operation time.[4–7] These superior electrical and chemical properties make the $LaGaO_3$ based oxide one of the most promising candidates as intermediate temperature electrolytes for SOFCs.

LSGM ceramics were mostly prepared by the conventional solid state reaction method.[4–8] The method suffers from time-consuming grinding and high temperature firing; and the synthesized powder is not chemically homogeneous and the particle size is large. LSGM ceramics have also been synthesized by other methods, such as sol–gel method,[9] Pechini method,[10,11] and combustion method.[12] Recently, Li et al. studied the preparation of $La_{0.85}Sr_{0.15}Ga_{0.85}Mg_{0.15}O_{2.85}$ by a PVA solution polymerization method and compared it with the solid state reaction method.[13] The method involves a mechanism of steric entrapment of cations into the polymer network, which prevents precipitation and thus ensures a homogeneous mixing at atomic level.[14] It was concluded that the PVA method was effective and efficient with pure perovskite phase produced at a much lower sintering temperature than the conventional ceramic

* Corresponding author. Tel.: +46 87908354; fax: +46 8216557.
E-mail address: shuail@kth.se (S. Li).

0955-2219/$ – see front matter © 2008 Elsevier Ltd. All rights reserved.
doi:10.1016/j.jeurceramsoc.2008.08.017

method, and this was attributed to the fine and homogeneous powders produced by the PVA method.

However, the secondary phases and microstructure of LSGM ceramics depend strongly on the synthesis methods and doping compositions,[15] and as a matter of fact, the synthesis of single perovskite phase is rather difficult. According to Huang et al., two secondary phases, namely $LaSrGaO_4$ and $LaSrGa_3O_7$, were identified in the sintered samples prepared by solid state reaction method.[7,8] While in a phase diagram study by Majewski et al., further secondary phases exist in the quaternary system La_2O_3–SrO–MgO–Ga_2O_3, e.g. $LaSrGaO_4$, $LaSrGa_3O_7$, MgO, Ga_2O_3, and $MgGa_2O_4$.[16] Moreover, the amounts of secondary phases in LSGM may not only relate to the synthesis route, but also depend on the dopants.[6] For example, when Sr and Mg were present together, it was found that the solubility of Sr and Mg in $LaGaO_3$ increased significantly.[16] Polini reported that the amount of secondary phases decreased with the increase of Mg at a given Sr content, while increased with the Sr content at a given Mg content.[11] The LSGM ceramics were mostly reported to have a microstructure with equiaxed grains.[8,11] Secondary phases, such as $LaSrGa_3O_7$ and MgO, could easily be identified in the SEM microstructures and were primarily accumulated along the grain boundaries. However, in a microstructure study of $LaGaO_3$ based electrolytes by Liu et al., secondary phases such as $LaSrGa_3O_7$ and $LaSrGaO_4$ existed with a rod shape in the perovskite phase matrix.[17]

In this work, we report a systematic study in which the relationship between doping composition and the secondary phases and microstructure was further investigated. To study the effect of Sr and Mg separately, $La_{1-x}Sr_xGa_{0.95}Mg_{0.05}O_{3-\delta}$ ($x = 0.05$–0.25) and $La_{0.8}Sr_{0.2}Ga_{1-y}Mg_yO_{3-\delta}$ ($y = 0.05$–0.20) were prepared by the PVA method. In order to get as pure perovskite phase as possible, the powders were calcined at temperature of 1300 °C.[10,11,13] The sintered pellets were characterised by X-ray diffraction, scanning electron microscope, as well as ac impedance spectroscopy. We also discuss the effect of doping content on the electrical properties of LSGM electrolytes, such as ionic conductivity and activation energy.

2. Experimental

2.1. Materials and preparation

The powders were synthesized using the following nitrate salts as cation sources: $La(NO_3)_3{\cdot}6H_2O$ (99.99%), $Sr(NO_3)_2$ (99.97%), $Ga(NO_3)_3{\cdot}xH_2O$ (99.9%) and $Mg(NO_3)_2{\cdot}6H_2O$ (99.97%) (all of them were from Alfa Aesar, a Johnson Matthey Company). The x value in the formula of gallium nitrate was determined to be 9 using a thermogravimetric analysis (TGA). Stoichiometric amounts of the given nitrate salts were mixed initially in distilled water and homogenized in a glass beaker. This solution was then mixed together with PVA solution in a glass beaker. The PVA solution was made by dissolving appropriate amount of PVA ($-(CH_2-CHOH)-_n$, molecular weight of 57,000–66,000, Alfa Aesar) into distilled water and stirring on a hot plate at 150 °C. The proportions of PVA to nitrate salts were adjusted in such way that the ratio of positively charged valences from metal cations to hydroxyl group of PVA is 1:1. For example, in the case of 1 mol $La_{0.9}Sr_{0.1}Ga_{0.95}Mg_{0.05}O_{2.925}$, total positively charged valences are 5.85 mol, and then the amount of PVA corresponding to 5.85 mol hydroxyl group is needed. The resulting precursor solution was stirred and homogenized on a hot plate for 1 h at room temperature. The solution was then heated at 250 °C to evaporate water while stirring. Black crisp char was finally formed and dried in an oven at 250 °C overnight. The char was ground into fine powder with an agate mortar and pestle. Calcination was subsequently performed in an air atmosphere in a tube furnace at 1300 °C for 3 h.

The as calcined powder was mixed with 1 wt.% PVA solution for binder and ground with an agate mortar and pestle. This powder was uniaxially pressed into pellets with 11 mm diameter and 2 mm thickness. The pressure was 200MPa. Green pellets were sintered at a temperature of 1470 °C for 20 h in air in a muffle furnace.

2.2. Characterisation

The phases in specimens were identified using X-ray Diffraction (XRD) (X'Pert Pro, PANalytical) with Cu Kα radiation. For the sintered samples, pellets were crushed into powders and then examined. The operating conditions for XRD were 45 kV, 40 mA at room temperature. Scans were taken in a 2θ range of 20–80° with a step size of 0.02°.

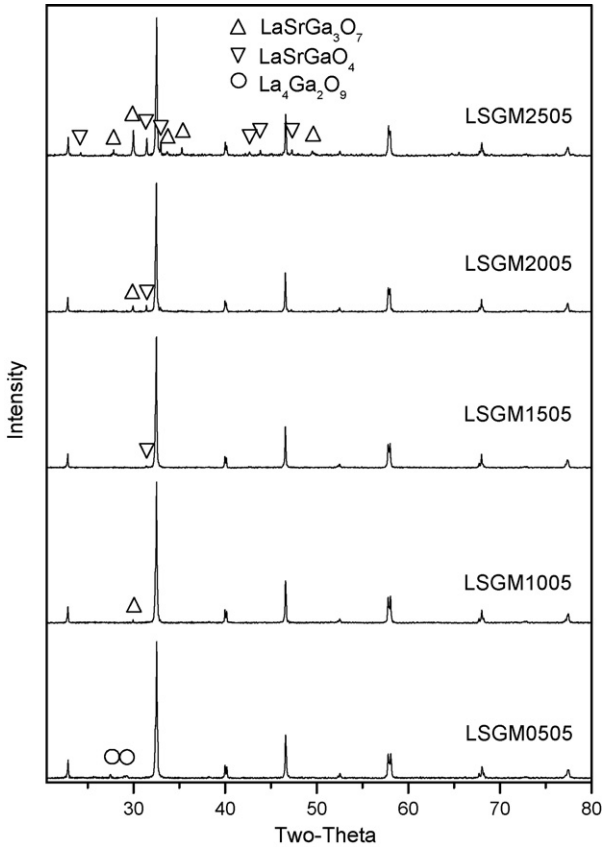

Fig. 1. XRD patterns of sintered $La_{1-x}Sr_xGa_{0.95}Mg_{0.05}O_{3-\delta}$ pellets ($x = 0.05$–0.25).

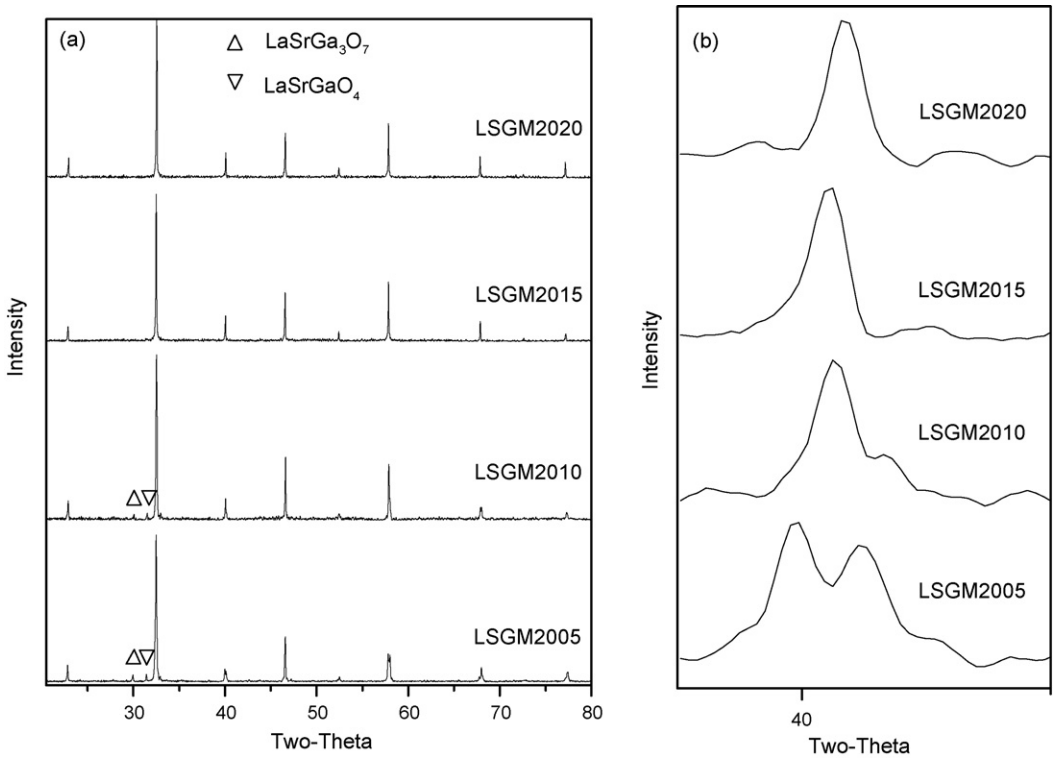

Fig. 2. (a) XRD patterns of sintered $La_{0.8}Sr_{0.2}Ga_{1-y}Mg_yO_{3-\delta}$ pellets ($y = 0.05$–0.20). (b) Enlarged XRD pattern portion around $2\theta = 40^\circ$ showing a change from orthorhombic to cubic symmetry.

The microstructures of sintered pellets were studied by scanning electron microscope (SEM) (JSM-840, JEOL). The pellets were wet-ground, polished and thermally etched at 1350 °C for 0.5 h. Chemical compositions were determined by an X-ray energy dispersive spectrometer (EDS) (Link, Oxford) attached to the SEM.

The ac conductivity of sintered pellets was obtained using two-probe impedance spectroscopy. Pellets were wet-ground to a thickness of about 1 mm. Gold paste (Agar Scientific) was applied on both sides of pellets and fired at 730 °C for 2 h. Measurements were made using electrochemical impedance spectroscopy (EI300, Gamry Instruments) over a frequency range of 300 kHz to 1 Hz in air. The temperature range was 500–800 °C at an interval of 50 °C. Pellets were kept at each temperature for at least 40 min to allow thermal equilibrium. Impedance from cablings, leads and sample holders were obtained by measuring a blank cell.

In this paper, $La_{1-x}Sr_xGa_{1-y}Mg_yO_{3-\delta}$ composition is referred to LSGM with numbers denoting contents of Sr and Mg. For example, $La_{0.8}Sr_{0.2}Ga_{0.9}Mg_{0.1}O_{2.85}$ is denoted as LSGM2010.

3. Results and discussion

3.1. X-ray diffraction patterns

Fig. 1 shows the XRD patterns of the sintered $La_{1-x}Sr_xGa_{0.95}Mg_{0.05}O_{3-\delta}$ ($x = 0.05$–0.25) pellets. Diffraction peaks from the perovskite phase are found in the LSGM pellets, illustrating that $LaGaO_3$ perovskite is essentially formed after sintering. The peak splitting at around $2\theta = 40^\circ$ shows the structure to be noncubic and the samples could be indexed with the orthorhombic $LaGaO_3$ (JCPDS 24-1102). Fig. 2 shows the XRD patterns from sintered $La_{0.8}Sr_{0.2}Ga_{1-y}Mg_yO_{3-\delta}$ ($y = 0.05$–0.20) pellets. These samples are also characterised with perovskite phase after sintering. However, it is interesting to note that the sintered samples with a fixed Sr content of 20 at.% have a structure change from orthorhombic to cubic with increasing Mg content. The enlarged portion of XRD patterns around $2\theta = 40^\circ$ for these samples are shown in Fig. 2(b). Sintered LSGM2005 has an orthorhombic symmetry, which is verified in Fig. 2(b) where two reflection peaks are identified. But the samples LSGM2015 and LSGM2020 have a cubic symmetry which is confirmed by the well defined (1 1 1) reflection peak. The peak splitting for sample LSGM2010 is not as much for sample LSGM2005, and this might reveal the

Table 1
Estimation of the amount of secondary phases in LSGM

Specimen	$LaSrGa_3O_7$ (%)		$LaSrGaO_4$ (%)		$La_4Ga_2O_9$ (%)	
	Calcined	Sintered	Calcined	Sintered	Calcined	Sintered
LSGM0505	1.4	0	0	0	6.1	2.4
LSGM1005	5.1	2.0	0	0	1.3	0
LSGM1505	10.9	0	5.8	1.3	3.3	0
LSGM2005	15.3	4.0	8.9	4.0	2.5	0
LSGM2505	25.6	14.1	14.1	9.3	1.7	0
LSGM2010	16.1	3.0	10.9	3.0	0	0
LSGM2015	13.5	0	11.0	0	0	0
LSGM2020	9.2	0	14.3	0	0	0

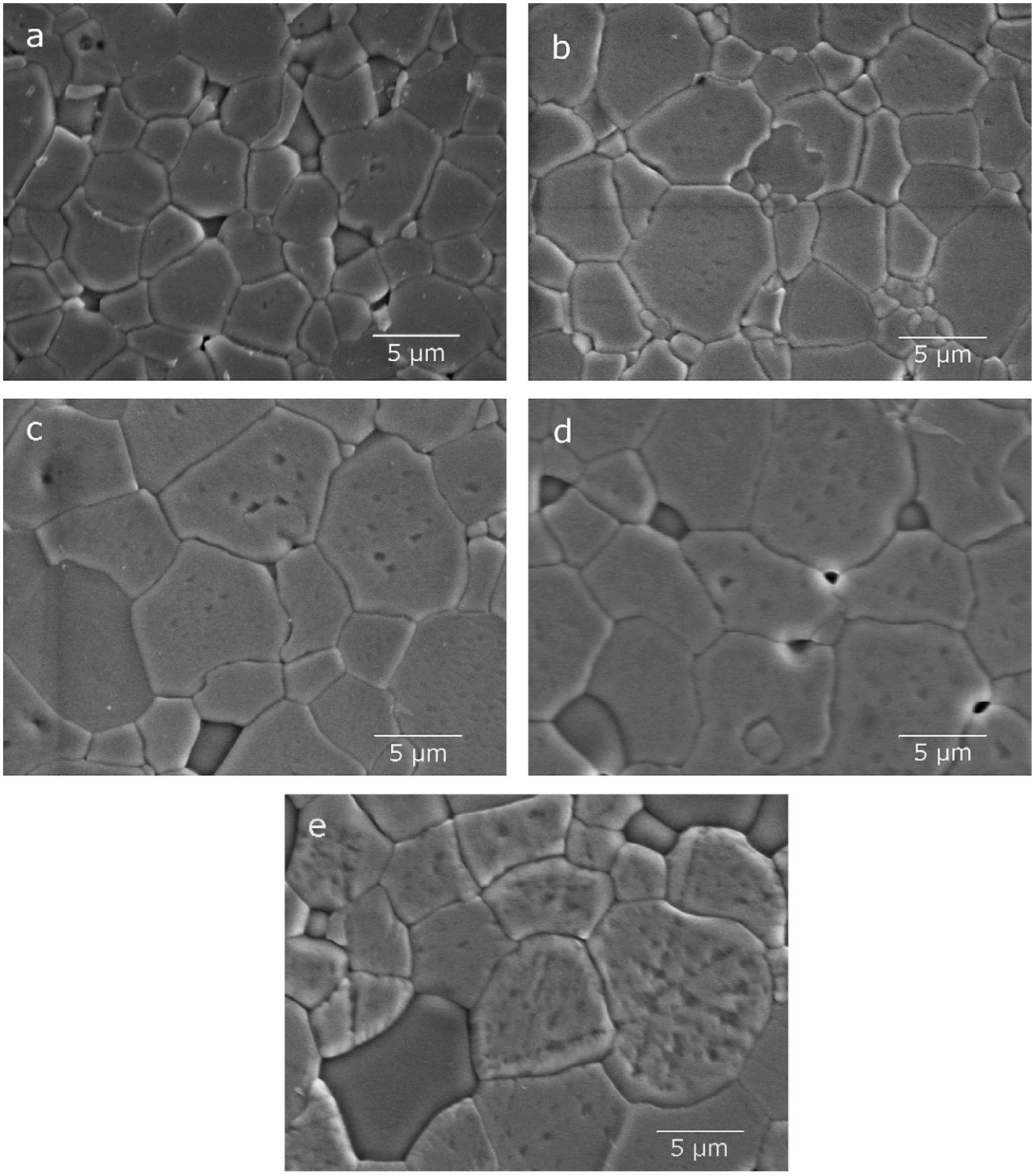

Fig. 3. SEM showing microstructures and secondary phases of $La_{1-x}Sr_xGa_{0.95}Mg_{0.05}O_{3-\delta}$, where $x = 0.05$–0.25: (a) LSGM0505, (b) LSGM1005, (c) LSGM1505, (d) LSGM2005, (e) LSGM2505.

fact that the sample has a mixture of orthorhombic and cubic structure. The crystal structure of LSGM strongly depends on the doping content and temperature. There are contradictory reports about the crystal structure of Sr and/or Mg doped $LaGaO_3$ perovskite.[5,6,7,18] Huang et al. reported a primitive cubic structure of $LaGaO_3$ at all doping levels of Sr and Mg.[7] However it was found in other works that the structure could change from orthorhombic to cubic with increasing content of dopants.[6,18] For example, Datta reported an orthorhombic structure for samples with total dopant content $x+y<0.25$, whereas a cubic symmetry for $x+y>0.35$ with either x or $y>0.2$. It is generally believed that the higher symmetry of the

crystal structure gives a better oxide ion conductivity and thus is preferable.[19]

Secondary phases in sintered samples are demonstrated in the XRD patterns in Figs. 1 and 2. These secondary phases are identified to be $La_4Ga_2O_9$ (JCPDS 53-1108), $LaSrGa_3O_7$ (JCPDS 45-0637) and $LaSrGaO_4$ (JCPDS 24-1208). Surprisingly, all the sintered samples of $La_{1-x}Sr_xGa_{0.95}Mg_{0.05}O_{3-\delta}$ with $x = 0.05$–0.25 have secondary phases (Fig. 1). Trace amount of secondary phases are detected in $La_{1-x}Sr_xGa_{0.95}Mg_{0.05}O_{3-\delta}$ with $x = 0.05$–0.20, while $La_{0.75}Sr_{0.25}Ga_{0.95}Mg_{0.05}O_{3-\delta}$ shows quite a lot of secondary phases. The solubility of Sr in $LaGaO_3$ is 10–20 at.% when Mg content is kept 5 at.%, as reported by various researchers.[6,7,16] So the solubility limit of Sr in $LaGaO_3$ does not reasonably explain the presence of these secondary phases. One of the possible reasons for the trace amount of secondary phases is maybe the short calcination time (3 h). It is believed that a higher calcination temperature or prolonged holding time may result in a pure sintered pellet. For instance, Tas et al. found that LSGM2017 prepared by a Pechini method contained 4–5 wt.% secondary phases even after calcination at 1400 °C for 6 h. It was reported that increasing calcination time or increasing firing temperature could remove these secondary phases effectively.[10] It is seen in Fig. 2 that the secondary phases are also identified in $La_{0.8}Sr_{0.2}Ga_{1-y}Mg_yO_{3-\delta}$ with $y = 0.05$–0.2, $LaSrGa_3O_7$ and $LaSrGaO_4$. However, as the Mg content increases, the amount of secondary phases decreases, and in particular, no secondary phase is detected in LSGM2015 and LSGM2020.

The amount of secondary phases is estimated by the ratio of the integrated intensity of the most intense peaks of the secondary phase over the perovskite $LaGaO_3$. This is a semi quantitative estimation of XRD patterns and reflects the relative amount of the secondary phases. Table 1 shows the amount change of secondary phases in calcined and sintered samples. All the powders suffer from secondary phases after calcination at 1300 °C. Except for low doping specimens, LSGM0505 and LSGM1005, calcined powders contain much secondary phases, >20% as shown in Table 1. The sintering process can the substantially reduce these secondary phases. The amount change of secondary phases in the sintered pellets with doping content is illustrative. At a Mg content of 5 at.%, the amount of secondary phases, such as $LaSrGa_3O_7$ and $LaSrGaO_4$, increases when the content of Sr increases. $LaSrGa_3O_7$ and $LaSrGaO_4$ are Sr rich compounds, so it is believed that excessive addition of Sr is compensated by formation of Sr rich secondary phases with increasing x value in $La_{1-x}Sr_xGa_{0.95}Mg_{0.05}O_{3-\delta}$. On the other hand when Sr is fixed to 20 at.%, there is a fast decrease of amount of Sr containing secondary phases as the Mg content increases. The solubility of Sr could be extended by the addition of Mg.

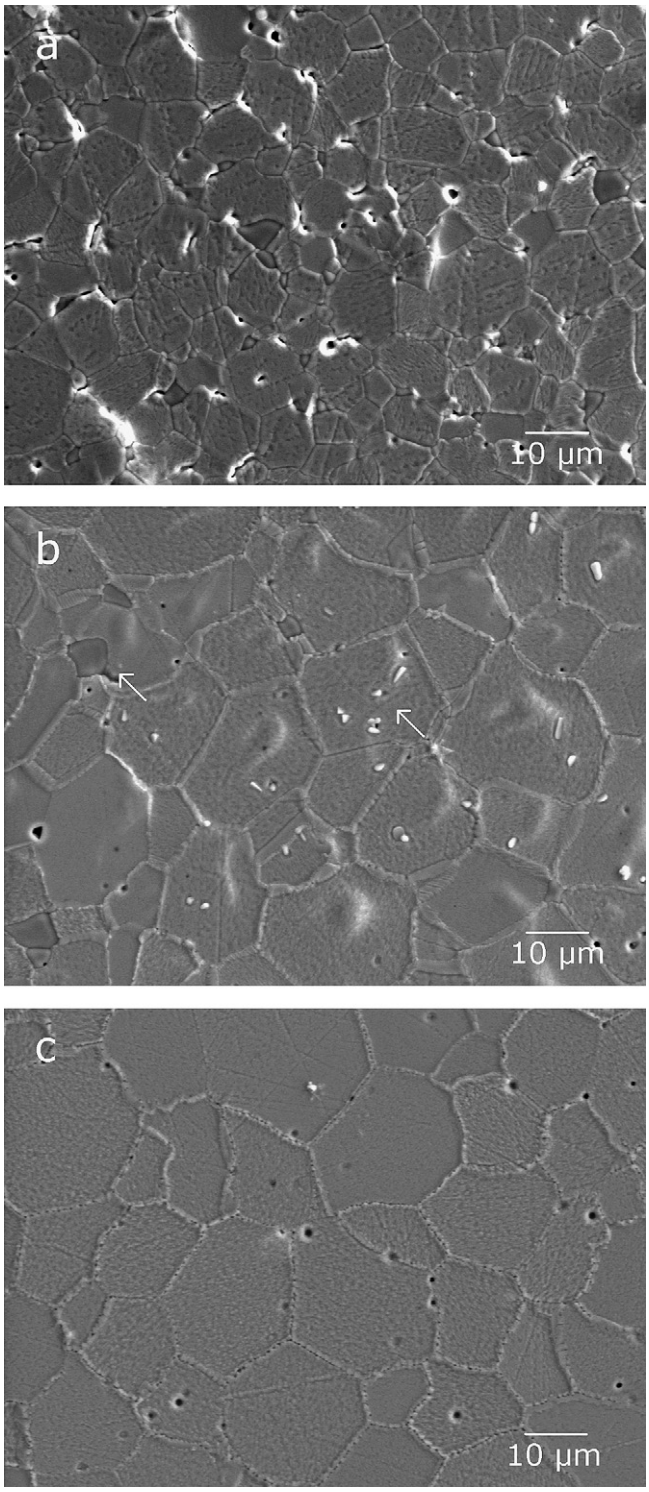

Fig. 4. SEM showing microstructures and secondary phases of $La_{0.8}Sr_{0.2}Ga_{1-y}Mg_yO_{3-\delta}$, where $y = 0.10$–0.20: (a) LSGM2010, (b) LSGM2015, (c) LSGM2020.

3.2. Microstructure

The SEM microstructures of $La_{1-x}Sr_xGa_{0.95}Mg_{0.05}O_{3-\delta}$ ($x = 0.05$–0.25), polished and thermally etched at 1350 °C, are shown in Fig. 3. Equiaxed microstructure with no abnormal grain growth is demonstrated. The pellets are dense and with few pores. Increasing Sr content results in bigger grains, but this is not apparent with high Sr doping content. However, SEM illustrates increasing grain sizes for $La_{0.8}Sr_{0.2}Ga_{1-y}Mg_yO_{3-\delta}$ ($y = 0.10$–0.20) pellets, as shown in Fig. 4. The reason for the larger average grain size (20–26 μm) in LSGM2015 and LSGM2020 could be the less secondary phases (Table 1). The

Density of all sintered pellets, as determined by the Archimedes method, is larger than 97% of theoretical density.

Secondary phases could be easily distinguished from the matrix perovskite phase in the microstructures as shown in Figs. 3 and 4. The dark grains accumulated along grain boundaries are secondary phases, $LaSrGa_3O_7$ or $La_4Ga_2O_9$, demonstrated by energy dispersive spectroscopy. Although LSGM2015 is found to be single $LaGaO_3$ perovskite by XRD, two secondary phases are clearly visible in the SEM microstructures, Fig. 4(b). The small amount of secondary phases is apparently beyond the detection limit of XRD. The dark intragranular secondary phase is found to be $LaSrGa_3O_7$ by EDS. While for the bright plate-like phase protruding from grain surface, the region is too small to perform EDS. Similar phenomenon was also reported by Abram et al. in a study of LSGM2017.[20] The authors attribute this plate-like phase to be $LaSrGaO_4$. This should not be the case in this work, because no such bright plate-like phase could be detected by SEM in those other samples containing $LaSrGaO_4$, as determined by XRD. Therefore, no $LaSrGaO_4$ could be found in the microstructures, even when it is detected by XRD. It has been reported that $LaSrGaO_4$ has a low melting point, ~1400 °C,[8] and should be in a liquid state at the sintering temperature of 1470 °C. The liquid phase $LaSrGaO_4$ may wet over grains, thus no detectable $LaSrGaO_4$ could be found in the microstructure. On the other hand, secondary phases, such as $LaSrGa_3O_7$ and $La_4Ga_2O_9$ have higher melting points, >1600 °C and ~1700 °C, respectively. They do not melt at the sintering temperature, and thus remain along grain boundaries. LSGM2020 has no secondary phase in the microstructure observation, which corresponds to the XRD analysis.

Few and uniformly distributed pores can be seen through the SEM microstructure. Detailed examination shows that the pores are mainly accumulated along grain boundaries. However, in LSGM2015 and LSGM2020, more pores are found and they are in both grain boundaries and grain bulks. Considering the much bigger grain sizes in these two pellets, the reason for this could be that these pores are trapped in the grains during the grain growth. The pores, whether in grain boundaries or grains, may deteriorate the electrical properties. They block the oxide ion migration, and thus decrease the ionic conductivity.

3.3. Electrical properties

Electrical properties of sintered samples are characterised using ac impedance spectroscopy (IS). Generally, impedance spectroscopy allows separation of bulk, grain boundary, and electrode processes of the ceramics.[21] A typical impedance spectroscopy of ceramics normally resolves three parts, a bulk semicircle, a grain boundary semicircle, and an electrode arc. Huang et al. investigated the grain boundary effect in LSGM using impedance spectroscopy.[8] It was reported that $LaSrGa_3O_7$ along the grain boundary is oxide ion insulating and contributes a depressed grain boundary semicircle in the impedance spectroscopy. While Abram et al. discussed the effect from $LaSrGaO_4$ secondary phase within LSGM2017 grains, using a more quantitative approach to model the IS data with equivalent

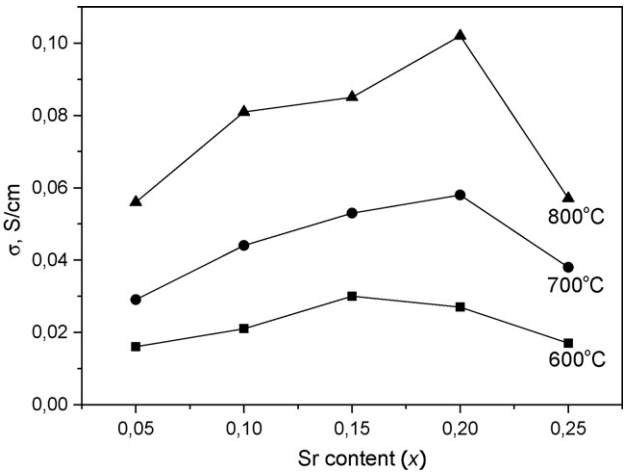

Fig. 5. The conductivity of $La_{1-x}Sr_xGa_{0.95}Mg_{0.05}O_{3-\delta}$ as a function of Sr content.

electrical circuit.[20] The equivalent circuit is rather difficult to assess, and the authors demonstrated the importance of correct equivalent circuit to extract physically significant parameters. In this work, simple hand fitting procedure to measure total resistance from impedance complex plane (Z' vs Z'') is used.

Fig. 5 shows the total conductivity of $La_{1-x}Sr_xGa_{0.95}Mg_{0.05}O_{3-\delta}$ ($x = 0.05$–0.25) at 600 °C, 700 °C and 800 °C, respectively. At a Mg level of 5 at.%, the conductivity increases with Sr content to a maximum at $x = 0.15$ for 600 °C and $x = 0.20$ for 700 °C and 800 °C. At different temperatures, the highest conductivity occurred at different contents. This reflects a different dependence of conductivity activation energy on composition. LSGM2505 has an inferior electrical conductivity, which apparently has much to do with the large amount of secondary phases in the sintered pellets (see Table 1). As shown in Fig. 6, the ionic conductivity increases with increasing Mg content initially, and decreases after reaching a maximum. LSGM2010 has the highest conductivity at 800 °C, $\sigma = 0.128$ S/cm, which is comparable to literature values.[5,6] According to Huang et al., the highest conductivity at 800 °C ($\sigma = 0.17$ S/cm) was observed for LSGM2017 prepared by a solid state reaction method.[7] However, it was reported that LSGM with $x + y = 0.35$ had the highest conductivity in another

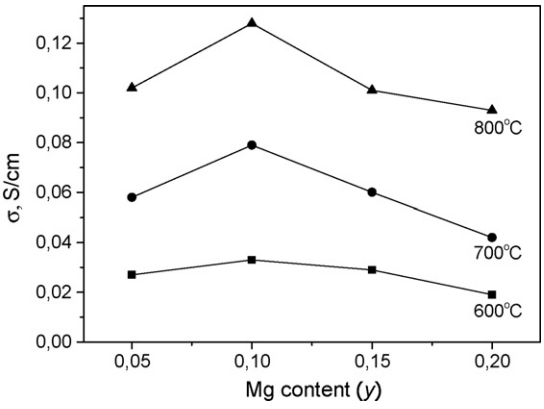

Fig. 6. The conductivity of $La_{0.8}Sr_{0.2}Ga_{1-y}Mg_yO_{3-\delta}$ as a function of Mg content.

Table 2
Electrical properties of LSGM pellets

Pellet	Total conductivity (S/cm)			ln A	E (eV)	E (eV)*	E (eV)**
	600 °C	700 °C	800 °C				
LSGM0505	0.016	0.029	0.056	9.908	0.547	N/A	0.634
LSGM1005	0.021	0.044	0.081	10.875	0.597	0.87	0.642
LSGM1505	0.030	0.053	0.085	10.218	0.524	0.918	0.624
LSGM2005	0.027	0.058	0.102	11.275	0.609	0.874	0.602
LSGM2505	0.017	0.038	0.057	10.565	0.590	N/A	0.615
LSGM2010	0.033	0.079	0.128	11.588	0.614	0.950	0.789
LSGM2015	0.029	0.060	0.101	11.384	0.617	1.06	0.785
LSGM2020	0.019	0.042	0.093	12.556	0.739	1.15	0.837

* Ref. 6.
** Ref. 7.

work.[6] This discrepancy is maybe caused by the different synthesis methods, microstructures and crystal structures of LSGM oxides. It should be pointed out that LSGM2010 pellet has trace amount of secondary phases according to the XRD analysis, although it has the highest ionic conductivity at 800 °C. So it is reasonable to expect that the conductivity could be higher if purer perovskite phase can be obtained for LSGM2010. LSGM2015 and LSGM2020 have inferior ionic conductivities, and even they are found to have purer perovskite phase. As shown in the microstructures (see Fig. 4), the amount of pores in these two samples is found to be higher than in other specimens, and they may block the oxygen ion migration as discussed above. The pores may thus be a deteriorating effect on the ionic conductivity for LSGM2015 and LSGM2020. Meanwhile, LSGM2015 and LSGM2020 microstructures show apparent thickening of grain boundaries, Fig. 4. This indicates a molten composition forms and wet over grains. This grain boundary thickening is probably amorphous and could be another reason for the inferior conductivity of LSGM2015 and LSGM2020.

Table 2 compares the electrical properties of sintered LSGM samples with various compositions. The Arrhenius plots for $La_{0.8}Sr_{0.2}Ga_{1-y}Mg_yO_{3-\delta}$ in the temperature range 500–800 °C are shown in Fig. 7. A linear relationship of conductivity with temperature was found. The conductivities of other samples are found to follow a similar linear relationship. Activation energies (E) for conductivities of all pellets are calculated from the Arrhenius plots and are listed in Table 2. The activation energy values are lower than the reported literature values.[6,7] The activation energy for LSGM consists of association energy (E_a) and migration energy (E_m), where E_a is the energy needed for dissociation of oxygen vacancies from their cation atmosphere, and E_m is the migration energy or mobility barrier for oxygen vacancies. At low temperatures both are present, but with increasing temperatures, there is an order–disorder transition at a critical temperature T^* and only the migration energy remains at elevated temperatures. Huang et al. reported the critical temperature to be 599 ± 49 °C.[7] It is thus reasonable to attribute the activation energy (E) to the migration energy (E_m) in our case. Therefore, the lower activation energy values in our work could be explained by a lower migration barrier. And the reason for this difference is probably related to lattice strain or mismatch introduced by different synthesis methods. The issue is complex and there is not yet a definite explanation to it. It is seen that further work is required to get a complete understanding of this phenomenon. Fig. 8 compares the activation energies of all samples. It is revealed that the activation energy increases with increasing content of Mg. However, there is no obvious trend with the increase of Sr content. This indicates that

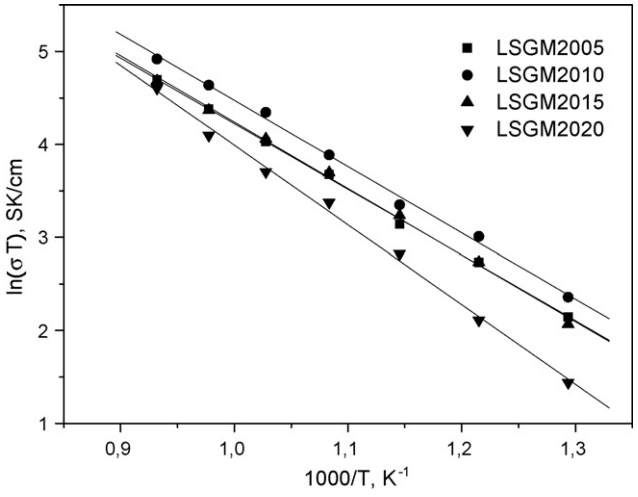

Fig. 7. Arrhenius plots for $La_{0.8}Sr_{0.2}Ga_{1-y}Mg_yO_{3-\delta}$ pellets.

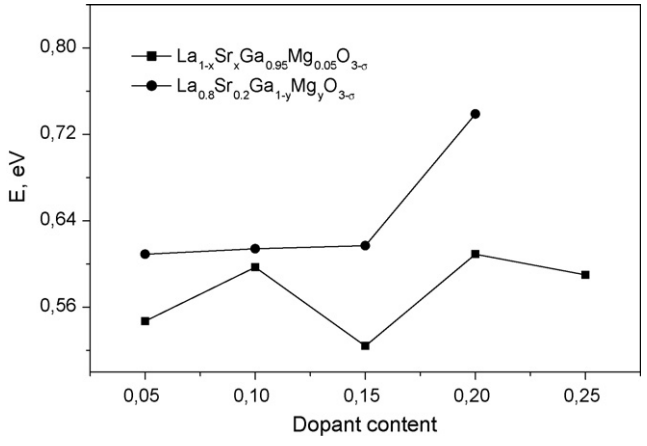

Fig. 8. The conductivity activation energy of LSGM as a function of dopant content.

the Mg addition increases the migration energy, while the Sr addition has no specific effect on the migration energy. Earlier calculations on the perovskite type oxides demonstrated that vacancy migration take place along the ⟨1 1 0⟩ edge of the anion octahedron.[22,23] In $LaGaO_3$, an oxygen atom forms two bonds both with Ga and La. Significant binding energies between Mg and oxygen vacancy was found compared with the near-zero binding energy for Sr and oxygen vacancy using a computer simulation.[23] This means that an oxygen vacancy is more strongly trapped by Ga–O–Mg pair than by the La–O–Sr pair. Therefore, addition of Mg has more effect on the migration barrier than Sr.

4. Conclusions

LSGM ceramics with various dopant contents were prepared using a PVA solution polymerization method. The crystal structure of the $LaGaO_3$ perovskite changes with increasing dopant content. $La_{1-x}Sr_xGa_{0.95}Mg_{0.05}O_{3-\delta}$ ($x = 0.05$–0.25) pellets could be characterised with orthorhombic symmetry. However, the sintered samples with fixed Sr content of 20 at.% showed a structure change from orthorhombic to cubic with the increase of Mg content. A cubic symmetry was observed for $La_{0.8}Sr_{0.2}Ga_{1-y}Mg_yO_{3-\delta}$ with $y \geq 15$ at.%. The secondary phases in pellets were mainly $LaSrGaO_4$, $LaSrGa_3O_7$ and $La_4Ga_2O_9$ as revealed by XRD analysis. The relative amount of these secondary phases was found to depend on dopant contents. The amount of Sr rich secondary phases, $LaSrGaO_4$ and $LaSrGa_3O_7$, increased with increasing Sr content, while enhanced solubility was observed when doping with Mg. SEM observation showed equiaxed grains in sintered samples. Secondary phases, such as $LaSrGa_3O_7$ and $La_4Ga_2O_9$, were confirmed by EDS and they were found to accumulate along grain boundaries. Because of the lower melting point of $LaSrGaO_4$, it was liquid at the sintering temperature of 1470 °C and wetting the grains. Thus no $LaSrGaO_4$ was detected in the SEM microstructures for all sintered pellets. Oxygen ionic conductivities were enhanced by doping with Sr and Mg. The activation energy increased with increasing content of Mg, while there was no specific trend with the Sr content. The highest ionic conductivity value $\sigma = 0.128$ S/cm at 800 °C was found for LSGM2010.

Acknowledgement

The authors would like to thank Prof. Zhi-Cheng Li from School of Materials Science and Engineering at Central South University (Hunan, China) for comments and suggestions on the early version of manuscript.

References

1. Minh, N. Q., Ceramic fuel cells. *J. Am. Ceram. Soc.*, 1993, **76**, 563–588.
2. George, R. A. and Bessette, N. F., Reducing the manufacturing cost of tubular SOFC technology. *J. Power Sources*, 1998, **71**, 131–137.
3. Fergus, J. W., Electrolytes for solid oxide fuel cells. *J. Power Sources*, 2006, **162**, 30–40.
4. Ishihara, T., Matsuda, H. and Takita, Y., Doped $LaGaO_3$ perovskite type oxide as a new oxide ionic conductor. *J. Am. Ceram. Soc.*, 1994, **116**, 3801–3803.
5. Feng, M. and Goodenough, J. B., A superior oxide-ion electrolyte. *Eur. J. Solid State Inorg. Chem.*, 1994, **31**, 663–672.
6. Huang, P. and Petric, A., Superior oxygen ion conductivity of lanthanum gallate doped with strontium and magnesium. *J. Electrochem. Soc.*, 1996, **143**, 1644–1648.
7. Huang, K., Tichy, R. S. and Goodenough, J. B., Superior perovskite oxide-ion conductor; strontium- and magnesium-doped $LaGaO_3$: I, phase relationships and electrical properties. *J. Am. Ceram. Soc.*, 1998, **81**, 2565–2575.
8. Huang, K., Tichy, R. S. and Goodenough, J. B., Superior perovskite oxide-ion conductor; strontium- and magnesium-doped $LaGaO_3$: II, ac impedance spectroscopy. *J. Am. Ceram. Soc.*, 1998, **81**, 2576–2580.
9. Huang, K., Feng, M. and Goodenough, J. B., Sol-gel synthesis of a new oxide-ion conductor Sr- and Mg-doped $LaGaO_3$ perovskite. *J. Am. Ceram. Soc.*, 1996, **79**, 1100–1104.
10. Tas, A. C., Majewski, P. J. and Aldinger, F., Chemical preparation of pure and strontium- and/or magnesium-doped lanthanum gallate powders. *J. Am. Ceram. Soc.*, 2000, **83**, 2954–2960.
11. Polini, R., Pamio, A. and Traversa, E., Effect of synthetic route on sintering behaviour, phase purity and conductivity of Sr- and Mg-doped $LaGaO_3$ perovskites. *J. Eur. Ceram. Soc.*, 2004, **24**, 1365–1370.
12. Cong, L., He, T., Ji, Y., Guan, P., Huang, Y. and Su, W., Synthesis and characterization of IT-electrolyte with perovskite structure $La_{0.8}Sr_{0.2}Ga_{0.85}Mg_{0.15}O_{3-\delta}$ by glycine-nitrate combustion method. *J. Alloys Compd.*, 2003, **348**, 325–331.
13. Li, Z., Zhang, H., Bergman, B. and Zou, X., Synthesis and characterization of $La_{0.85}Sr_{0.15}Ga_{0.85}Mg_{0.15}O_{3-\delta}$ electrolyte by steric entrapment synthesis method. *J. Eur. Ceram. Soc.*, 2006, **26**, 2357–2364.
14. Lee, S. J. and Kriven, W. M., Crystallization and densification of nano-size amorphous cordierite powder prepared by a PVA solution polymerization route. *J. Am. Ceram. Soc.*, 1998, **81**, 2605–2612.
15. Djurado, E. and Labeau, M., Second phases in doped lanthanum gallate perovskites. *J. Eur. Ceram. Soc.*, 1998, **18**, 1397–1404.
16. Majewski, P., Rozumek, M. and Aldinger, F., Phase diagram studies in the systems La_2O_3-SrO-MgO-Ga_2O_3 at 1350–1400 °C in air with emphasis on Sr and Mg substituted $LaGaO_3$. *J. Alloys Compd.*, 2001, **329**, 253–258.
17. Liu, N., Shi, M., Wang, C., Yuan, Y., Majewski, P. and Aldinger, F., Microstructure and ionic conductivity of Sr- and Mg-doped $LaGaO_3$. *J. Mater. Sci.*, 2006, **41**, 4205–4213.
18. Datta, P., Majewski, P. and Aldinger, F., Structural studies of Sr- and Mg-doped $LaGaO_3$. *J. Alloys Compd.*, 2007, **438**, 232–237.
19. Yao, W., Tang, Z., Zhang, Z., Luo, S., Li, J. and Tan, Q., Inter-relationship between crystal symmetry and ionic conductivity in doped $LaGaO_3$. *Mater. Sci. Eng. B*, 2003, **99**, 309–312.
20. Abram, E. J., Sinclair, D. C. and West, A. R., A strategy for analysis and modelling of impedance spectroscopy data of electroceramics: doped lanthanum gallate. *J. Electroceram.*, 2003, **10**, 165–177.
21. Bauerle, J. E., Study of solid electrolyte polarization by a complex admittance method. *J. Phys. Chem. Solids*, 1969, **30**, 2657–2670.
22. Kilner, J. A. and Brook, R. J., A study of oxygen ion conductivity in doped nonstoichiometric oxides. *Solid State Ionics*, 1982, **6**, 237–252.
23. Islam, M. S. and Davies, R. A., Atomistic study of dopant site-selectivity and defect association in the lanthanum gallate perovskite. *J. Mater. Chem.*, 2004, **14**, 86–93.